Research Square

Preprints are preliminary reports that have not undergone peer review.
They should not be considered conclusive, used to inform clinical practice,
or referenced by the media as validated information.

Precise Positioning of a Hoist Using Fuzzy PID Optimized by an Improved Particle Swarm Optimization Algorithm

Mingliang Yang
Taiyuan University of Science and Technology
Jiaming Xu
xujiaming0410@163.com

Taiyuan University of Science and Technology
Xijun Xu
Taiyuan Fortucky Logistics Equipment & Technology Co.,Ltd
Heng Yang
Taiyuan University of Science and Technology
Qing Dong
Taiyuan University of Science and Technology

Research Article

Keywords: chain-driven hoist, positioning accuracy, fuzzy PID control, particle swarm optimization, electromechanical co-simulation

Posted Date: November 16th, 2026

DOI: https://doi.org/10.21203/rs.3.rs-11374059/v1

License: This work is licensed under a Creative Commons Attribution 4.0 International License.
Read Full License

Additional Declarations: No competing interests reported.

Precise Positioning of a Hoist Using Fuzzy PID Optimized by an Improved Particle Swarm Optimization Algorithm

Mingliang Yang[1], Jiaming Xu[1*] ,Xijun Xu[2],Heng Yang[1],Qing Dong[1]
（1.School of Mechanical Engineering, Taiyuan University of Science and Technology, Taiyuan 030000, Shanxi, China）
(2. Taiyuan Fortucky Logistics Equipment & Technology Co.,Ltd,Taiyuan 030024, China)
Corresponding author: Jiaming Xu (1998-), male, M.S. candidate, specializing in intelligent control and precision positioning of mechanical systems. E-mail: xujiaming0410@163.com

Abstract: To address the problems of sluggish dynamic response and insufficient positioning accuracy in long-travel chain-driven hoists operating under variable-load and high-inertia conditions, a precision positioning strategy based on fuzzy PID control optimized by an Improved Particle Swarm Optimization (IPSO) algorithm is proposed. First, a multibody dynamic model of the hoisting system is established in Adams to investigate the influence of rigid-flexible coupling characteristics associated with long-travel chain transmission on end-positioning performance. Second, to overcome the overshoot and steady-state error commonly encountered with conventional control methods under complex operating conditions, a fuzzy PID controller is developed in Simulink, and the IPSO algorithm is introduced to efficiently optimize the key controller parameters. Finally, an Adams-Simulink electromechanical co-simulation platform is established for performance verification. Comparative simulations are conducted among the conventional fuzzy PID controller, the standard PSO-optimized fuzzy PID controller, and the proposed IPSO-optimized fuzzy PID controller. The results show that the proposed method achieves faster closed-loop convergence and significantly reduces the settling time, while effectively improving the end-positioning accuracy and overall control performance of the hoist under complex operating conditions.

Keywords: chain-driven hoist; positioning accuracy; fuzzy PID control; particle swarm optimization; electromechanical co-simulation

1 Introduction

With the rapid development of intelligent manufacturing and modern logistics, high-density warehousing systems have been widely adopted because of their high space utilization. As a core vertical conveying device in warehousing systems, the operating performance of a hoist directly affects the overall throughput efficiency. In practical applications, long-travel hoists are often required to operate under complex conditions characterized by high operating speeds and substantial load variations, placing stringent demands on the final positioning accuracy of the load platform. However, owing to the inherent polygonal effect of chain drives, the rigid-flexible coupling associated with long-travel transmission, and nonlinear disturbances induced by high-inertia loads, the hoist is prone to dynamic lag and positioning deviations when

approaching the target position. These effects can significantly reduce the reliability of pick-and-place operations and the overall system performance.

For positioning control of hoisting systems, conventional PID control is structurally simple, but it is often difficult to simultaneously achieve fast response, low overshoot, and high steady-state accuracy in mechanical systems with time-varying parameters and strong nonlinearities. Improved fuzzy PID control has been shown to enhance the dynamic performance of crane positioning and anti-sway control[1]. Variable-universe and multi-parameter self-tuning mechanisms can further improve position control and load anti-sway performance[2]. For conveying systems with time-varying and nonlinear characteristics, fuzzy PID control can also improve the dynamic response of the system[3]. Therefore, incorporating fuzzy logic into PID control can enhance the controller's adaptability to complex operating conditions; however, the selection of fuzzy-control parameters and rule bases still depends, to some extent, on engineering experience.

To reduce the dependence of fuzzy PID parameter tuning on manual experience, intelligent optimization algorithms have increasingly been employed for controller-parameter optimization. The use of particle swarm optimization to tune fuzzy PID parameters can improve response speed, overshoot suppression, and steady-state performance[4]. Dynamically adjusting the inertia weight and learning parameters of the particle swarm can improve the search performance of the algorithm and the robustness of the control system[5]. Combining particle swarm optimization with fuzzy inference can further integrate PID parameter optimization with online adaptive adjustment[6].

To address these technical limitations, the conventional particle swarm optimization (PSO) algorithm is improved in this study and combined with a fuzzy PID control strategy. To better balance the global exploration capability of PSO with its local search capability in the later stages of optimization, dynamic inertia-weight and particle-velocity constraint strategies can be introduced during parameter optimization[7]. On this basis, a dynamically decreasing inertia-weight mechanism is adopted together with particle-velocity constraints and position-boundary limits to perform offline optimization of the key fuzzy PID controller parameters, thereby reducing the uncertainty associated with manual tuning.

First, a multibody dynamic model of the hoisting system incorporating the principal physical nonlinearities is established in Adams. A closed-loop control system is then developed in Simulink, and the parameter-compensation strategy obtained through IPSO is integrated into the fuzzy PID controller. Finally, Adams-Simulink electromechanical co-simulation is carried out to evaluate the system's dynamic response, overshoot suppression capability, and final positioning performance under different load levels and lifting strokes. The results indicate that the proposed IPSO-fuzzy PID composite control strategy can effectively improve the positioning-control performance of the hoist, providing a theoretical basis and engineering reference for high-precision positioning control of long-travel hoisting systems.

2 Multibody Dynamic Modeling of the Hoist

A conventional continuous hoist has a highly complex mechanical configuration. In this study, the physical prototype is reasonably simplified in Adams, as illustrated in Fig. 1. Because the dominant transmission path associated with positioning deviations occurs during the vertical lifting stage, the original four-chain closed-loop circulation system is simplified to a unidirectional vertical lifting configuration. Meanwhile, the support frame is modeled as a rigid structure fixed to ground, and the dynamic-response analysis focuses on the principal transmission components, including the drive shaft, sprockets, chains, and load platform.

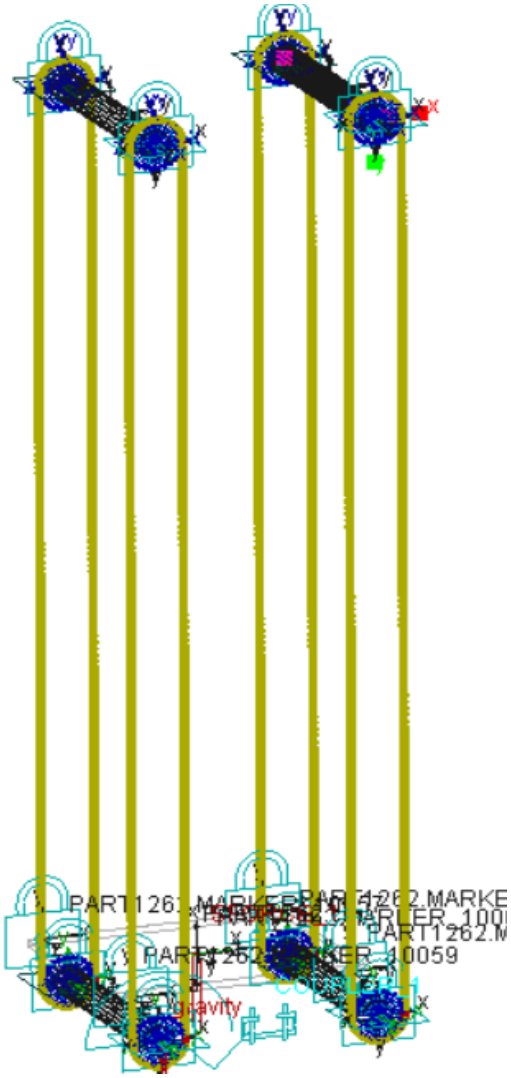


Fig. 1. Simplified model of the hoisting mechanism

2.1 Theoretical Analysis of the Dynamic Equivalence of Structural Simplification

To justify simplifying the complex four-chain circulation loop into a unidirectional vertical lifting structure and treating the support frame as a rigid body fixed to ground, this subsection provides a theoretical analysis from the perspectives of energy conservation in the dynamic system and reduction of nonessential degrees of freedom.

2.1.1 Justification for Treating the Support Frame as Rigid

The support frame of the physical prototype possesses a certain degree of elasticity. However, this study primarily focuses on the low-frequency, large-displacement motion of the load platform in the vertical direction, whereas the elastic deformation of the support frame has a comparatively small influence on the dominant motion. Therefore, the support frame is approximated as rigidly fixed to ground during modeling to reduce the number of model degrees of freedom and the associated computational complexity.

2.1.2 Mathematical Equivalence Analysis of Multi-Branch Constraints

The original system has a complex closed-loop topology consisting of multiple chains, in which the load platform is synchronously driven by four chain branches. It is assumed that the four chains have identical geometric and physical properties. The tensile stiffness of the vertical segment of each chain is denoted by $k_i(i = 1,2,3,4)$, and its damping coefficient is denoted by c_i. Under the drive condition in which the main shaft lifts the platform vertically, the load platform undergoes large-displacement motion only in the vertical direction, defined as the z-axis, while horizontal translation and sway are constrained by the guide rails.

According to the Lagrange equation, the generalized dynamic equation of the system in the vertical direction can be expressed as：

$$\frac{d}{dt}\left(\frac{\partial T}{\partial \dot{z}}\right) - \frac{\partial T}{\partial z} + \frac{\partial V}{\partial z} + \frac{\partial D}{\partial \dot{z}} = Q_Z \tag{1}$$

where

T is the total kinetic energy of the system, given by $T = \frac{1}{2}M\dot{z}^2 + \sum\frac{1}{2}J_j\dot{\theta_j}^2$, where M is the total mass of the load platform and payload, and J_j and θ_j are the rotational inertia and angular displacement, respectively, of the transmission shafts and sprockets;

V is the total potential energy of the system, including gravitational potential energy and the elastic strain energy of the chains;

D is the Rayleigh dissipation function, mainly associated with chain damping; and

Q_Z is the generalized force produced by nonconservative forces, i.e., the vertical driving force equivalent to the input torque applied to the main shaft.

The rigid-flexible coupling characteristics of the multi-chain system are primarily reflected in the axial tensile stiffness k_i and damping coefficient c_i. During upward motion of the load platform, the four chains form a parallel stiffness topology in the direction of motion because of the symmetry of the four loops. Therefore, the total tensile stiffness K_{total} and the total equivalent damping C_{total} satisfy

$$K_{total} = \sum_{i=1}^{4} k_i = 4k_i \tag{2}$$

$$C_{total} = \sum_{i=1}^{4} c_i = 4c_i \tag{3}$$

In the simplified unidirectional vertical lifting model, the physical parameters of the original four chains are equivalently aggregated. Let the equivalent translational stiffness and damping coefficient of the simplified lifting structure be $K_{eq} = K_{total}$ and $C_{eq} = C_{total}$, respectively. The equivalent potential energy V_{eq} and dissipation function D_{eq} of the simplified system are then given by

$$V_{eq} = Mgz + \frac{1}{2}K_{eq}\Delta z^2 = Mgz + \frac{1}{2}(4k_i)\Delta z^2 \tag{4}$$

Substituting the equivalent quantities T, V_{eq}, and D_{eq} into the Lagrange equation yields a vertical dynamic governing equation that is mathematically identical in form to that of the original four-loop closed-chain topology.

The model simplification adopted in this study preserves the total system mass, total driving torque, and equivalent axial tensile stiffness and damping, while eliminating non-primary degrees of freedom associated with unloaded loops that do not contribute to end positioning. Under the condition that the total mass, driving torque, and equivalent stiffness and damping in the vertical direction remain unchanged, the simplified model retains the principal dynamic characteristics of the vertical motion considered in this study while reducing the number of model degrees of freedom and the computational cost of the coupled simulation.

2.2 Hoist Parameter Settings

The simplified model consists of one drive shaft, three transmission shafts, eight sprockets, four chains, and one load platform. The upper limits of the equipment parameters are specified as a lifting height of 10 m and a maximum design payload of 300 kg. To emphasize the long-travel chain-transmission and control characteristics while reducing the influence of shaft elasticity on the end-positioning analysis, both the drive shaft and the transmission shafts are modeled as rigid shafts with a diameter of 60 mm and a length of 1200 mm. These dimensions are used solely as simulation-modeling parameters and are not intended to represent the final strength-based shaft design for an engineering implementation.

After the drive shaft is established, two roller-chain sprockets are generated on each shaft using the Machinery module in Adams, with all sprockets assigned identical

geometric parameters. The inner width between the inner plates of the chain is set to 15.75 mm, and the number of sprocket teeth is set to 25. Because the sprockets automatically generated by Adams use default dimensions corresponding to a smaller specification, the pitch diameter, outside diameter, and root diameter are recalculated according to the selected roller-chain parameters. For a chain pitch of p = 25.4 mm and a roller diameter of d_r =15.88mm, the pitch diameter is

$$d = \frac{p}{\sin(\pi \div z)} = \frac{25.4}{\sin 7.2} \approx 202.66mm \tag{5}$$

The outside diameter is calculated as

$$d_a = p(0.60 + \cot(\pi \div z)) \approx 216.30mm \tag{6}$$

The root diameter is calculated as

$$d_f = d - d_r = 202.22 - 15.88 = 186.78mm \tag{7}$$

The calculated dimensions are then entered into the sprocket-parameter interface to generate the sprockets. The resulting sprocket parameters are summarized in Table 1.

Table 1. Sprocket parameters

Number of teeth	Pitch diameter (mm)	Outside diameter (mm)	Root diameter (mm)	Pitch (mm)
25	202.66	216.30	186.78	25.4

During chain generation, the chain is parameterized so that the simulation model can represent chain-link deformation and impact during lifting. The chain pitch is set to 25.4 mm, consistent with the pitch of the drive sprocket; the inner width between the inner plates is 15.75 mm; and the roller diameter is 15.88 mm, which defines the contact geometry between the chain rollers and the sprocket tooth surfaces. The half-height of the chain plate is set to 10.5 mm for defining the chain-link geometry and center-of-mass location. The equivalent translational stiffness of the chain-link connection is set to 1.0×10^5 N/mm to represent the equivalent elastic behavior of the connection under tensile loading. The equivalent damping coefficient of the chain-link connection is set to 800.0 N·s/mm to characterize energy dissipation during impact, reversal, and meshing. These stiffness and damping values are equivalent parameters used in the Adams chain-transmission connection model and should not be interpreted as the overall axial stiffness and damping of the entire long chain.

With respect to system constraints and boundary conditions, a revolute joint is defined between the drive shaft and ground, each sprocket is rigidly connected to its

corresponding shaft, and the transmission shafts are synchronized through coupler constraints, as shown in Fig. 2. The load platform is modeled as the end effector and is connected as a rigid body to the four flexible transmission chains. Considering that the platform consists of a load-carrying deck, a supporting frame, and chain-connection components, an equivalent platform mass of 60 kg is assigned in the dynamic model, together with the corresponding center-of-mass location and moments of inertia determined from its geometry. The Adams gravitational field is activated throughout the model, with the gravitational acceleration set to g = 9.81 m/s² in the vertically downward direction, so that the self-weight of the platform is automatically incorporated into the system dynamic equations through its mass properties.

Rather than representing the payload by applying a constant external force at the center of mass of the platform, the payload is modeled as an additional mass rigidly attached to the platform. Two payload cases, 100kg and 200kg, are considered in the subsequent co-simulations, corresponding to 33.3% and 66.7% of the maximum design payload, respectively. Including the 60kg platform mass, the corresponding total moving masses are 160kg and 260kg. This modeling approach allows changes in payload mass to be reflected simultaneously in both the gravitational loading and the acceleration/deceleration inertial response, thereby providing a more physically representative description of the hoist dynamics under variable-load and long-travel operating conditions.

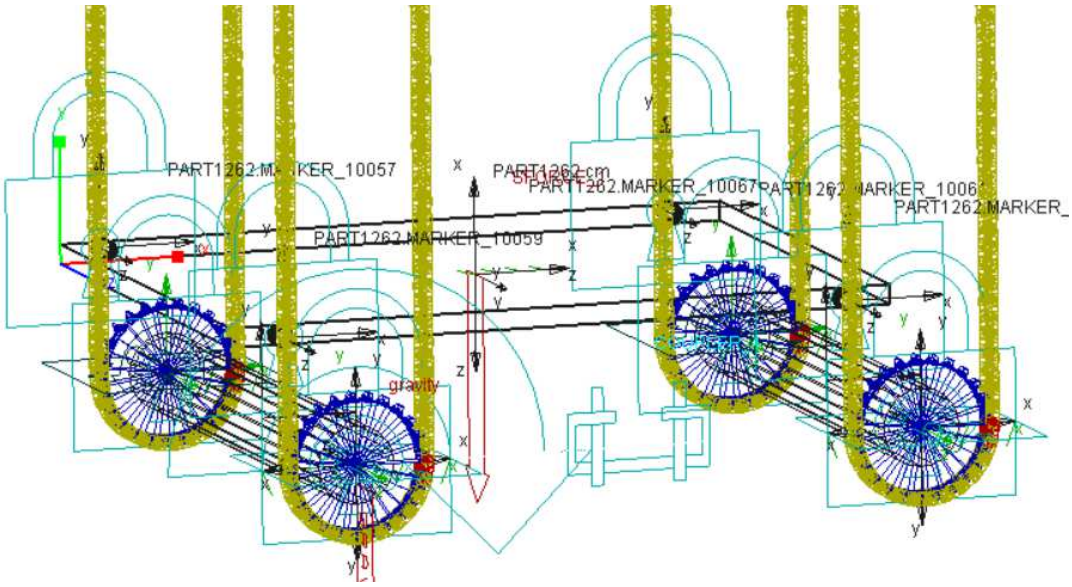


Fig. 2. Schematic diagram of the model constraints

3 Adaptive Fuzzy PID Controller Design

The fuzzy PID controller uses the system error and its rate of change as input variables and adjusts the PID control parameters in real time through fuzzy inference, enabling the controller to adapt to changes in the system operating state. This error- and error-rate-based fuzzy self-tuning structure can dynamically modify the control parameters according to the current system state and thereby improve position-control performance[2]. The overall structure of the fuzzy PID control system adopted in this

study is shown in Fig. 3.

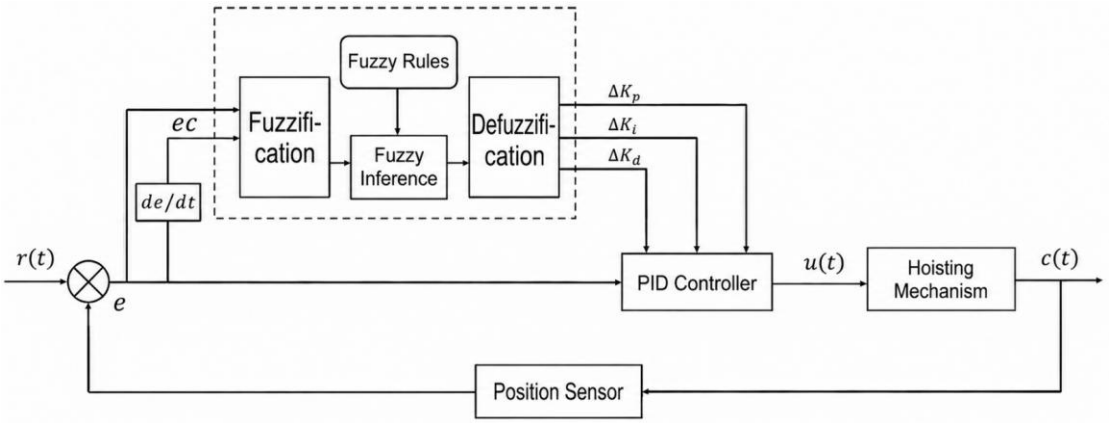


Fig. 3. Block diagram of the fuzzy PID control system

In the block diagram, $r(t)$ denotes the reference input and $c(t)$ denotes the actual feedback response. Their difference defines the tracking error e(t), while the derivative of the error, i.e., its rate of change, is denoted by ec. In addition, ΔK_p, ΔK_i, and ΔK_d represent the dynamic correction increments of the PID gains, and $u(t)$ is the final control output.

The fuzzy PID controller operates as follows. The system continuously acquires the tracking error e and its rate of change ec as two input variables. These inputs are first fuzzified to determine their membership degrees in the corresponding fuzzy sets. Fuzzy inference is then performed according to the predefined rule base to obtain the correction quantities ΔK_p, ΔK_i, and ΔK_d. These correction quantities are subsequently used to adjust the PID parameters online, yielding the final output of the fuzzy PID controller, $u(t)$.

$$u(t) = (K_{p0} + \Delta K_p)e + (K_{i0} + \Delta K_i)\int_0^t edt + (K_{d0} + \Delta K_d)\frac{d_e}{d_t} \tag{8}$$

where K_{p0}, ΔK_i, and ΔK_d are the initial proportional, integral, and derivative gains of the PID controller, respectively.

3.1 Selection of Variables and Definition of Universes of Discourse

The displacement error e and its rate of change ec are selected as the input variables of the fuzzy controller, while the PID gain correction terms ΔK_p, ΔK_i, and ΔK_d are selected as the output variables. The fuzzy sets of both the input and output variables are uniformly partitioned into seven linguistic levels: {NB, NM, NS, ZO, PS, PM, PB}, corresponding to negative big, negative medium, negative small, zero, positive small, positive medium, and positive big, respectively. For computational consistency, the universes of discourse of the input and output variables are all normalized to the interval [−3, 3]. For illustration, the membership functions of the displacement error e are shown in Fig. 4.

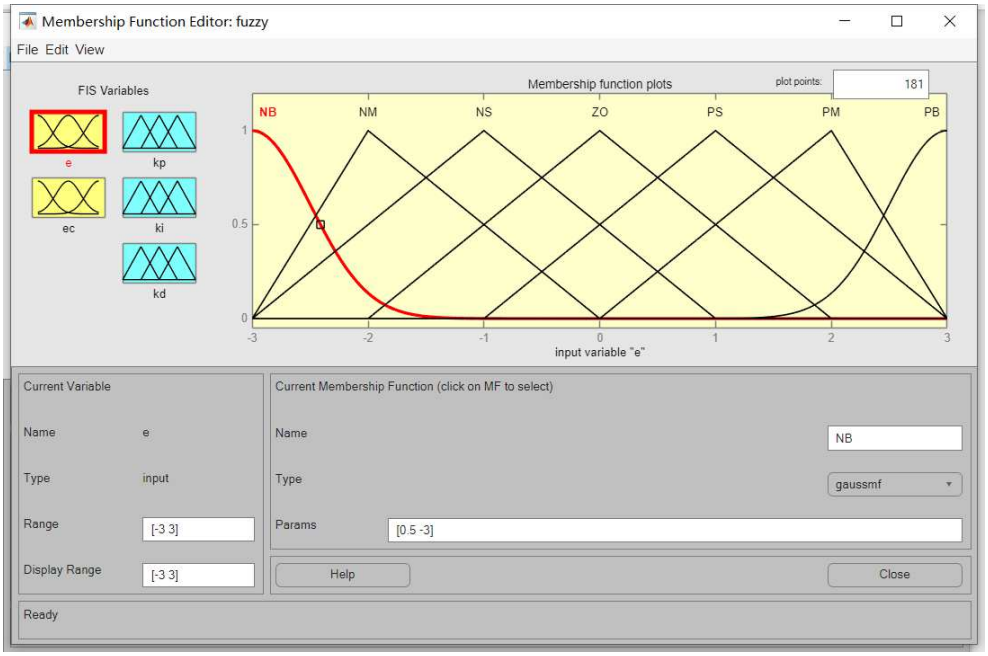


Fig. 4. Membership functions of the displacement error e

3.2 Establishment of Fuzzy Control Rules

The fuzzy rule base plays a critical role in determining controller performance and is formulated according to the following control principles. When the system error e is large, the correction term ΔK_p should be assigned a relatively large value so that the error can be rapidly suppressed and its magnitude reduced as a priority. When the system error e becomes small, ΔK_p should be reduced to limit overshoot while maintaining error suppression, thereby improving the stability of the closed-loop response. Since both the positioning error e and the error-rate variable ec are divided into seven fuzzy subsets, each of the three output variables ΔK_p, ΔK_i, and ΔK_d is governed by a 7 × 7 rule table containing 49 fuzzy rules, as shown in Fig. 5.

e	e_c						
	NB	NM	NS	ZO	PS	PM	PB
NB	PB/NB/PS	PB/NB/NS	PM/NM/NB	PS/NM/NB	PS/NS/NB	ZO/ZO/NM	ZO/ZO/PS
NM	PB/NB/PS	PB/NB/NS	PM/NM/NB	PS/NS/NM	PS/NS/NM	ZO/ZO/NS	NS/ZO/ZO
NS	PM/NB/ZO	PM/NM/NS	PM/NS/NM	PS/NS/NM	ZO/ZO/NS	NS/PS/NS	NS/PS/ZO
ZO	PM/NM/ZO	PM/NM/NS	PS/NS/NS	ZO/ZO/NS	NS/PS/NS	NM/PM/NS	NM/PM/ZO
PS	PS/NM/ZO	PS/NS/ZO	ZO/ZO/ZO	NS/PS/ZO	NS/PS/ZO	NM/PM/ZO	NM/PB/ZO
PM	PS/ZO/PB	ZO/ZO/NS	NS/PS/PS	NM/PM/PS	NM/PM/PS	NM/PB/PS	NB/PB/PB
PB	ZO/ZO/PB	ZO/ZO/PM	NS/PS/PM	NM/PM/PM	NM/PM/PS	NB/PB/PS	NB/PB/PB

Fig. 5. Fuzzy control rules for ΔK_p, ΔK_i, and ΔK_d

4 Optimization Algorithm Design

When intelligent optimization is applied to a fuzzy PID controller, different

quantities may be selected as optimization variables according to the specific control objective, including the PID gains, quantization factors, scaling factors, or fuzzy rules. Optimization of fuzzy PID parameters using particle swarm optimization (PSO) can improve the dynamic response of the control system[4]. In this study, the PID gain correction terms generated by the fuzzy PID controller are selected as the optimization variables, and an intelligent search procedure is employed to obtain more appropriate compensation values for the proportional, integral, and derivative gains.

During practical vertical conveying operations, long-travel flexible chain transmission can introduce time-varying system characteristics and nonlinear disturbances. To address the limitations associated with fixed scaling factors in conventional fuzzy controllers and their limited ability to accommodate such complex disturbances, a data-driven intelligent optimization mechanism is introduced. The error characteristics of the load platform during operation are collected, and the improved particle swarm optimization algorithm is used to determine a suitable set of control parameters offline. By replacing subjective empirical tuning with algorithm-based optimization, this strategy helps improve the dynamic adaptability of the system during acceleration and deceleration and enhances end-positioning performance. The corresponding operating principle is illustrated in Fig. 6.

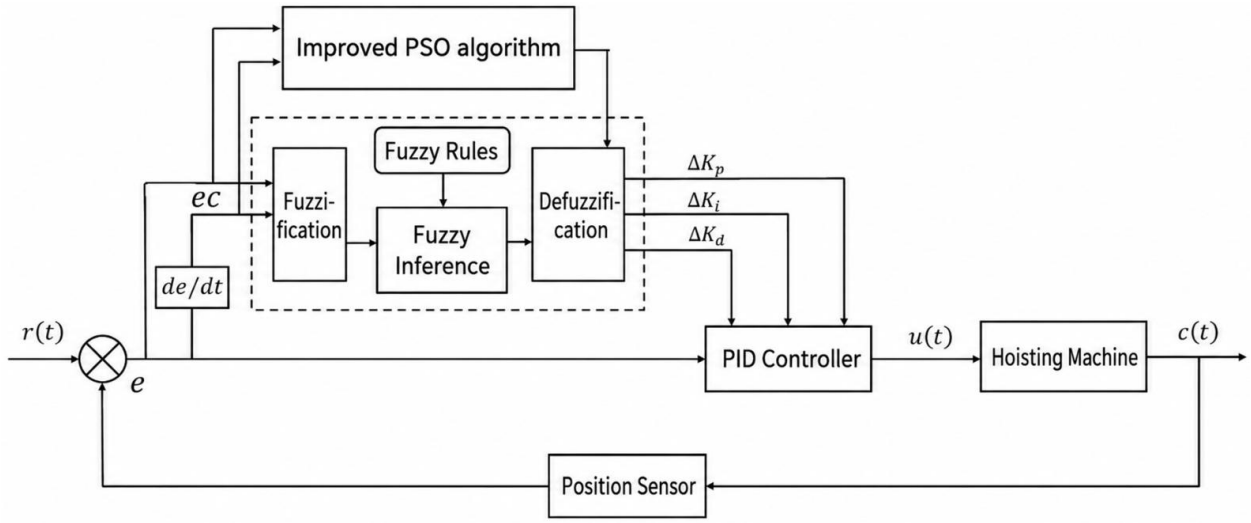


Fig. 6. Schematic diagram of the PSO-based fuzzy PID controller

4.1 Improved Particle Swarm Optimization Algorithm

In a conventional fuzzy PID control structure, the PID gain correction terms constitute key controller adjustment variables, and their values directly affect the transient response and steady-state control accuracy of the system. However, the parameters of conventional fuzzy PID controllers are commonly tuned on the basis engineering experience. Under complex operating conditions involving long travel, variable loads, and rigid-flexible coupling in the hoisting system, fixed parameter settings may fail to maintain consistent control performance and can lead to relatively large dynamic errors during end-positioning.

To reduce the uncertainty associated with manual tuning, particle swarm optimization is introduced into the fuzzy PID parameter optimization process. Particle swarm optimization (PSO), proposed in 1995, updates the velocity and position of each particle under the joint guidance of its personal best position and the global best position of the swarm, thereby enabling optimization in a continuous parameter space[8]. Nevertheless, standard PSO may have difficulty balancing global exploration and local exploitation in complex parameter spaces. Dynamically adjusting the inertia weight and learning parameters can improve the adaptability of the PSO search process[5]. Accordingly, in this study, the inertia weight as well as the velocity and position boundaries of standard PSO are modified to suit the parameter optimization requirements of the fuzzy PID controller for the hoist.

The static parameter compensation obtained using IPSO is combined with the dynamic correction generated by the fuzzy controller so that both terms jointly act on the PID gains, allowing the controller to integrate intelligent parameter optimization with online adaptive adjustment[6]. The search domain is defined as a three-dimensional parameter space, and the position vector of the i-th particle is expressed as $x_i = [CK_p,\ CK_i,\ CK_d]$ where CK_p, CK_i, and CK_d denote the correction terms for the proportional, integral, and derivative gains, respectively. Through iterative updates of particle velocity and position, the algorithm searches the parameter space for an optimal combination of correction terms, enabling the fuzzy PID controller to obtain more appropriate control parameters under different operating states of the hoist and thereby reduce end-positioning error and improve positioning accuracy.

On this basis, a composite parameter correction model integrating the conventional PID controller, dynamic fuzzy adjustment, and static compensation optimized by IPSO is formulated as follows:

$$K_p = K_{p0} + \Delta K_p + CK_p \tag{9}$$

$$K_i = K_{i0} + \Delta K_i + CK_i \tag{10}$$

$$K_d = K_{d0} + \Delta K_d + CK_d \tag{11}$$

where K_{p0}, K_{i0}, and K_{d0} are the initial parameters of the conventional PID controller; ΔK_p, ΔK_i, and ΔK_d are the dynamic correction terms generated online by the fuzzy logic controller according to the instantaneous system error and its rate of change; and CK_p, CK_i, and CK_d are the static PID parameter compensation terms obtained through offline optimization using the improved particle swarm optimization (IPSO) algorithm.

By combining the static compensation obtained through IPSO with the real-time dynamic adjustment of the fuzzy PID controller, the proposed controller integrates offline global search with online adaptive regulation, thereby improving the positioning performance of the hoist under variable-load conditions and nonlinear disturbances.

4.2 Dynamically Decreasing Inertia Weight Mechanism.

Standard PSO generally employs a fixed or predefined inertia weight, making it difficult to simultaneously maintain strong global exploration in the early optimization stage and effective local exploitation in the later stage. A relatively large inertia weight allows particles to retain larger search steps and thus explore a wider parameter space, but it may reduce local search accuracy in the later iterations. Conversely, a smaller inertia weight facilitates fine search around promising regions but may weaken global exploration during the early iterations. To address this trade-off, a dynamically decreasing inertia weight mechanism is adopted in this study, together with particle velocity and position boundary constraints, to improve standard PSO.

To provide stronger global exploration at the beginning of the search while enhancing local search accuracy in the later stage, the inertia weight is designed to decrease progressively with the iteration number $\omega(k)$:

$$\omega(k) = \omega_{max} - \frac{\omega_{max} - \omega_{min}}{k_{max}} \times k \tag{12}$$

where $\omega_{\max}$ and $\omega_{\min}$ are the maximum and minimum inertia weights, set to 0.9 and 0.4, respectively; k is the current iteration number; and $k_{\max}$ is the maximum number of iterations, set to 50 in this study.

As the optimization proceeds, the inertia weight gradually decreases from a relatively large value, causing both the particle search step and search range to contract progressively. This enables a smooth transition from global exploration in the early stage to refined local search in the later stage. The mechanism helps reduce large particle oscillations during the later iterations and improves the stability and local search accuracy of PID parameter optimization.

4.3 Multiple Boundary Constraints on Particle Velocity and Position

During PSO-based parameter optimization, an excessively large particle displacement in a single iteration may cause the particle to leave the effective search region rapidly. Limiting particle velocity restricts the search step in each iteration and reduces the likelihood of rapid deviation from the feasible parameter region[7]. Because out-of-range PID gain correction terms may lead to divergence of the Simulink closed-loop system and may also compromise the stable operation of the Adams mechanical model, additional boundary constraints are imposed on both particle position and velocity. The following hard boundary limits are applied:

$$x_{id}^{k+1} = \begin{cases} X_{max}, & x_{id}^{k+1} > X_{max} \\ X_{min}, & x_{id}^{k+1} < X_{min} \\ x_{id}^{k+1}, & \end{cases} \tag{13}$$

$$v_{id}^{k+1} = \begin{cases} X_{max}, & v_{id}^{k+1} > X_{max} \\ X_{min}, & v_{id}^{k+1} < X_{min} \\ v_{id}^{k+1}, & \end{cases} \tag{14}$$

During the iterative search, whenever a particle parameter exceeds the prescribed upper or lower bound, the algorithm forcibly clips and resets it to the corresponding boundary value. This operation prevents unsuitable parameter values from adversely affecting the electromechanical co-simulation system and improves the efficiency with which the algorithm screens PID gain correction terms.

Accordingly, the standard velocity and position update equations of the improved IPSO algorithm are written as

$$v_{id}^{k+1} = \omega(k) v_{id}^{k} + c_1 r_1 \left(pbest_{id} - x_{id}^{k}\right) + c_2 r_2 \left(gbest_{d} - x_{id}^{k}\right) \tag{15}$$

$$x_{id}^{k+1} = x_{id}^{k} + v_{id}^{k+1} \tag{16}$$

where $pbest_{id}$ denotes the historical best position of the individual particle; $gbest_d$ denotes the global best position of the swarm; c_1 and c_2 are the learning factors; and r_1 and r_2 are random variables uniformly distributed over the interval [0, 1].

4.4 Design of the Optimization Objective Function

The fitness function provides the criterion that guides the evolutionary search. To comprehensively evaluate the dynamic tracking error and end-positioning performance of the hoist during operation, the integral of time-weighted absolute error (ITAE) is adopted as the basic performance index. Because the end-positioning process is particularly sensitive to position overshoot, a penalty term for the maximum position overshoot is further incorporated into the ITAE criterion, resulting in the following composite objective function:

$$F = \int_0^T t|e(t)|dt + \alpha \cdot \sigma_{max} \tag{17}$$

where T is the duration of the electromechanical co-simulation; $e(t)$ denotes the instantaneous vertical position error of the load platform; $\sigma_{\max}$ is the maximum position overshoot of the system; and α is the overshoot-penalty weighting coefficient, which is set to 1000 in this study.

This objective function imposes a stringent engineering constraint on overshoot. If a particle, corresponding to a specific combination of PID gain correction terms, causes the hoist to pass beyond the target position as it approaches the destination, i.e.,

produces a nonzero σ_{max}, the penalty term substantially increases the resulting fitness value even when the earlier transient response is fast. Because the optimization process seeks to minimize the objective function, this penalty mechanism reduces the competitiveness of parameter combinations associated with pronounced overshoot and guides the swarm toward parameter regions that provide a better compromise among low overshoot, reduced oscillation, and fast response.

5 Adams-Simulink Co-Simulation

Co-simulation between multibody dynamics software and a control-system simulation platform enables bidirectional data exchange between the mechanical system response and the controller output, and has been applied to integrated dynamic and control analyses of hoisting machinery[9]. In this study, the multibody dynamic model of the hoist is established in Adams. An external control interface is created using Adams/Controls and coupled with the IPSO-based fuzzy PID controller implemented in MATLAB/Simulink to form a closed-loop electromechanical co-simulation system.

First, an external control interface is defined in the Adams multibody dynamic model of the hoist. The interface includes both input and output signals. The driving torque applied to the main shaft is defined as the input variable of the plant and is used to receive the control command $u(t)$ generated by the Simulink controller. The actual vertical displacement of the load-platform center of mass is defined as the output variable and is fed back to Simulink in real time as the feedback signal of the closed-loop system.

After the interface variables are defined, the Adams/Controls module is used to export a script containing the physical characteristics of the mechanical system. The exported model is then converted in MATLAB into an Adams subsystem, denoted as adams_sub, as shown in Fig. 7.

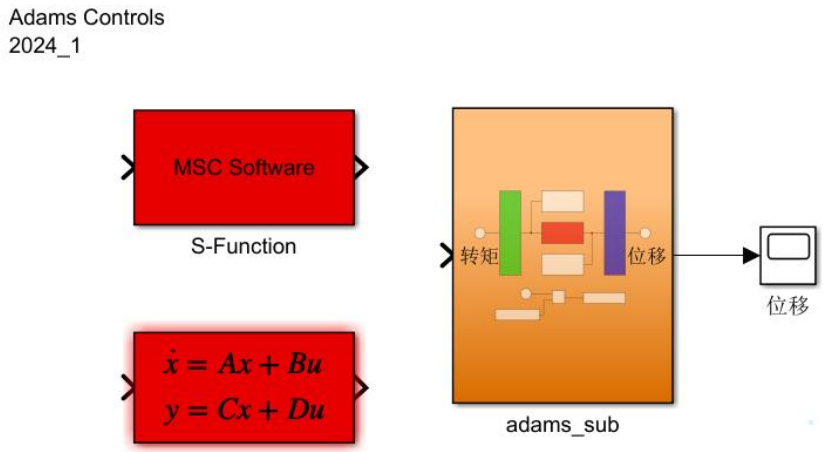


Fig. 7. ADAMS_sub simulation subsystem

In the Simulink environment, the Adams dynamic model, the fuzzy PID controller, and the IPSO optimization module are connected to form the closed-loop architecture shown in Fig. 8. During the simulation procedure, the IPSO algorithm performs offline parameter optimization according to the error characteristics associated with the prescribed operating condition. The resulting optimized compensation values are then loaded into the fuzzy PID controller. This completes the construction of the closed-loop electromechanical co-simulation platform.

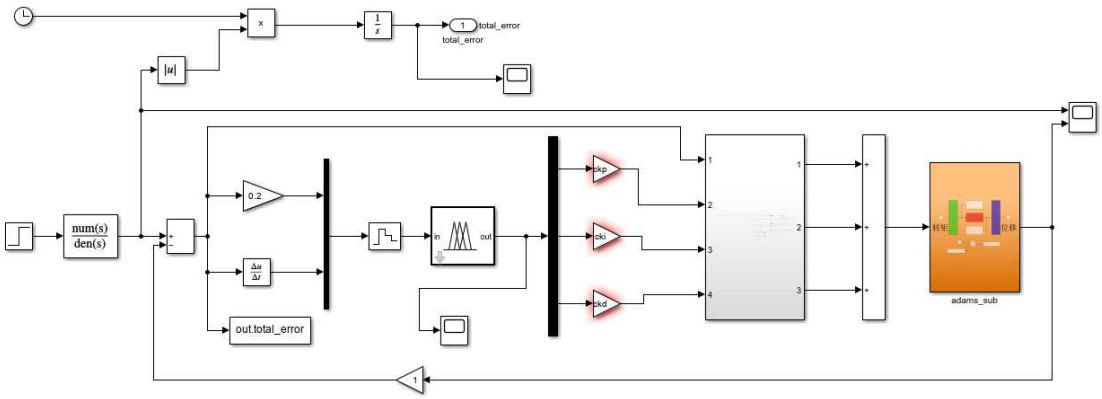


Fig. 8. MATLAB/Simulink simulation model of the controller

5.1 Simulation Parameter Settings

To evaluate the effectiveness of the proposed control strategy, a low-level implementation of the improved particle swarm optimization (IPSO) algorithm was developed in the MATLAB/Simulink environment. The initial swarm size was set to 30, and the maximum number of iterations was set to k_{max} =50. The maximum and minimum values of the dynamically decreasing inertia weight were set to $\omega_{\max} = 0.9$ and $\omega_{min} = 0.4$, respectively, and the learning factors were set to $c_1 = c_2 = 2$ to promote stable convergence during the later stages of the optimization. To further suppress position overshoot and oscillation during end-positioning, the overshoot-penalty weight in the composite objective function was set to 1000. The position and velocity bounds of the optimization variables are listed in Table 2. Whenever a particle exceeded the prescribed safety limits during an update, boundary clipping and reset were applied to maintain stable operation of the Adams-based closed-loop electromechanical co-simulation platform.

Table 2 Position and velocity bounds for the optimization variables

Optimization variable	Position lower bound X_{min}	Position upper bound X_{max}	Velocity lower bound V_{min}	Velocity upper bound V_{max}
CK_p	-10	50	-5	5
CK_i	-0.5	5	-0.5	0.5
CK_d	-1	10	-1	1

5.2 Simulation Results and Analysis

After the simulation parameters were specified, two co-simulation cases were

considered. In Case 1, the target lifting height was 5m, the added payload mass was 100kg, the load-platform mass was 60kg, and the total moving mass was 160kg. In Case 2, the target lifting height was 8m, the added payload mass was 200kg, and the total moving mass was 260kg. Except for the target lifting distance and payload mass, the mechanical configuration, controller structure, and IPSO algorithm settings were kept unchanged. Offline parameter optimization was performed separately for each operating condition to obtain the corresponding static PID compensation parameters. In both cases, a uniform gravitational field was applied in Adams so that the masses of both the load platform and the payload contributed to the gravitational and inertial dynamics.

After completion of the co-simulations, the optimization histories of the PID gain correction terms and the particle-swarm fitness values were obtained for both operating conditions. For the 5m, 100 kg payload case, the optimization history of the parameter correction terms is shown in Fig. 9, and the corresponding particle-swarm iteration history is shown in Fig. 10. After 50 IPSO iterations, the optimal compensation terms converged to $CK_p = 4.3821$, $CK_i = 0.0345$, and $CK_d = 4.1254$, while the best fitness value converged steadily to 14.8542. The multiple boundary constraints effectively prevented parameter excursions from causing divergence of the Simulink model and contributed to a stable optimization process.

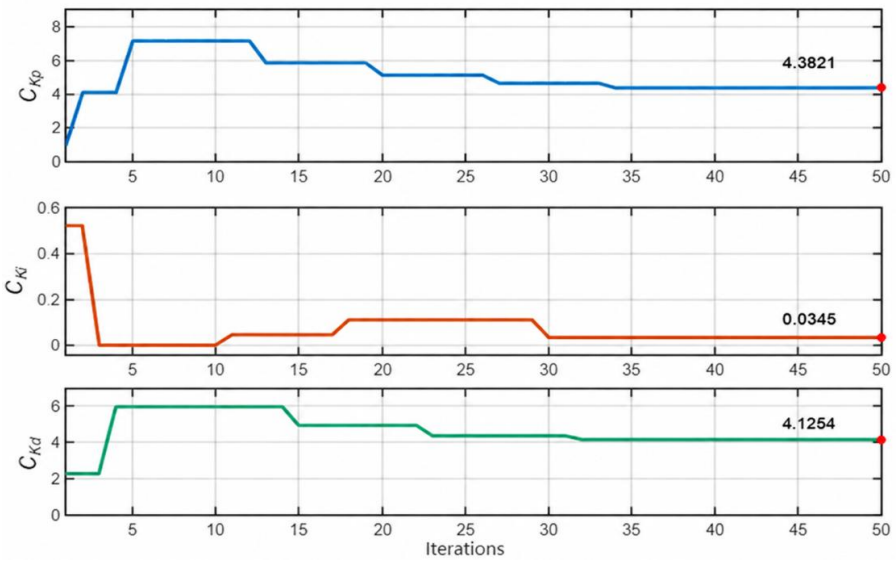


Fig. 9. Optimization curves of parameter adjustments for the 5 m travel condition

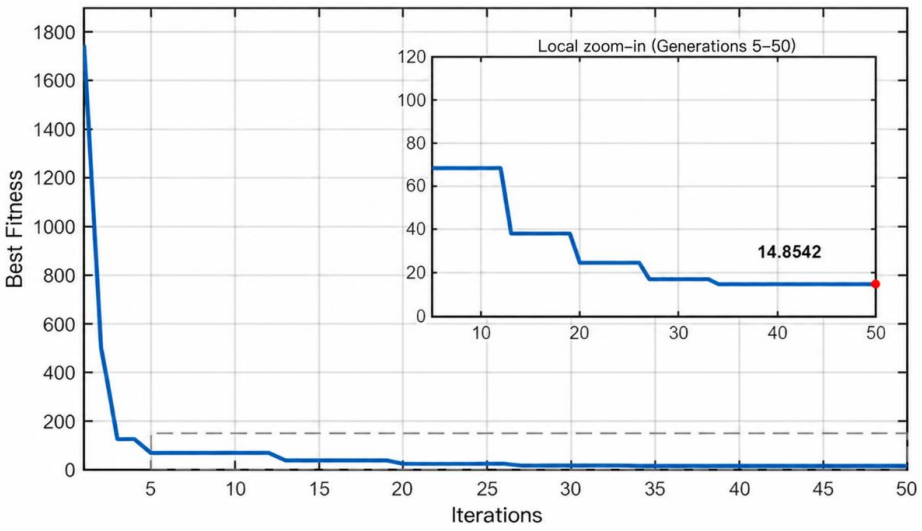


Fig. 10. PSO iteration curve for the 5 m travel condition

The optimization histories for the 8m case are presented in Fig. 11, while the corresponding iteration history is shown in Fig. 12. During the early stage of the optimization (approximately the first 10 iterations), the relatively large inertia weight enabled rapid exploration of the global search space, and the values of CK_p, CK_i, and CK_d exhibited comparatively large variations. As the number of iterations increased, the inertia weight decreased according to the prescribed dynamic schedule, causing the particle search range to contract gradually and the swarm to move toward a more promising parameter region. By approximately the 30th iteration, the three parameters had largely stabilized. At the 50th iteration, a favorable parameter combination within the prescribed search domain was obtained: $CK_p = 4.1526$, $CK_i = 0.0183$, and $CK_d = 2.4571$. Meanwhile, the best fitness value decreased rapidly during the early iterations and ultimately converged to 11.3524, indicating that parameter combinations associated with undesirable overshoot had been effectively screened out.

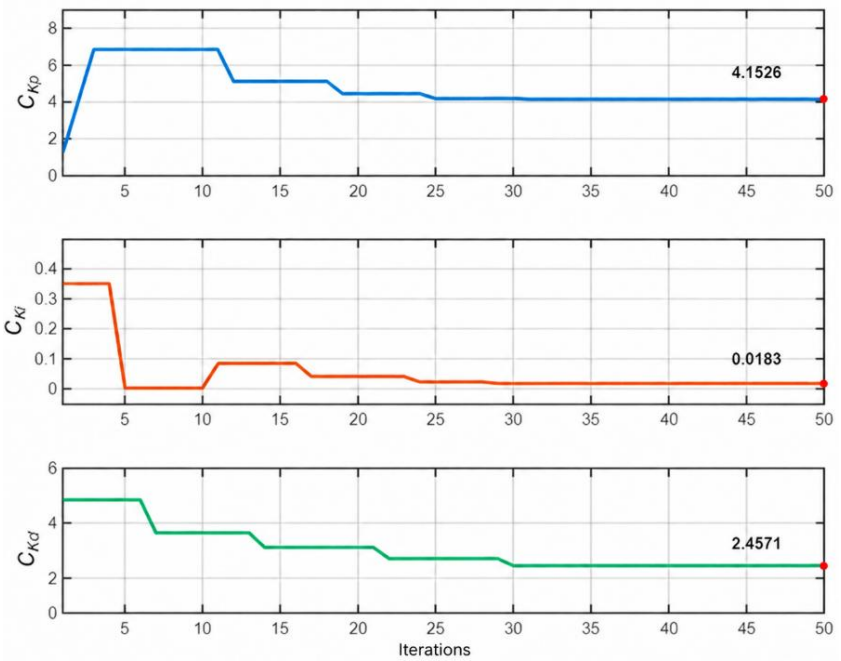


Fig. 11. Optimization curves of parameter adjustments for the 8 m travel condition

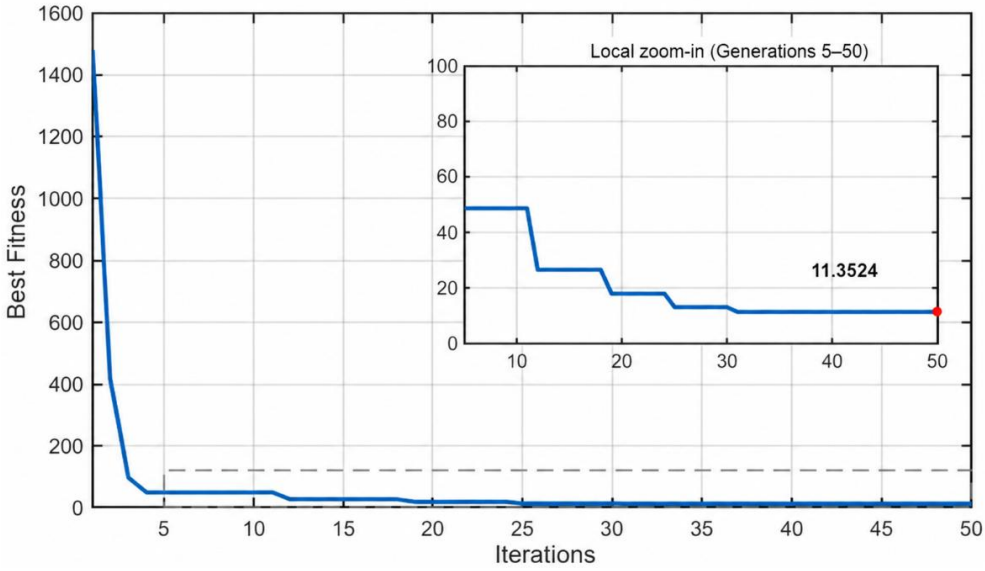


Fig. 12. PSO iteration curve for the 8 m travel condition

5.3 Dynamic Performance Analysis

To further evaluate the influence of different control strategies on the end-positioning performance of the hoist, the maximum position overshoot distance and steady-state positioning error are introduced in addition to settling time and percentage overshoot as performance indices. The instantaneous positioning error of the load platform is defined as

$$e(t) = r - y(t) \tag{18}$$

where r is the target lifting position and $y(t)$ is the actual displacement of the load platform. For a response exhibiting position overshoot, the maximum position overshoot distance is defined as

$$e_{os} = M_p r \tag{19}$$

where M_p denotes the position overshoot ratio. When no overshoot occurs, $e_{os} = 0$. To evaluate end-positioning accuracy after the system has entered the steady state, the steady-state positioning error is defined as the mean absolute difference between the actual and target positions over a stable time interval immediately before the end of the simulation:

$$e_s = \frac{1}{\Delta T} \int_{T-\Delta T}^{T} |r - y(t)| dt \tag{20}$$

where T is the total simulation time and ΔT is the time window used for steady-state error evaluation. In this study, the final 1s of the simulation is selected as the

steady-state evaluation interval. Because the vertical axes of the available displacement-response plots are given on the meter scale, millimeter-level residual errors cannot be resolved reliably. Accordingly, the steady-state positioning error is estimated only qualitatively from the response curves; an accurate millimeter-level value would require the original Adams-Simulink displacement data.

The displacement responses for the 5m and 8m operating conditions show that all three control strategies gradually converge to the target position toward the end of the simulation. No obvious steady-state position deviation can be identified at the resolution of the current plots; therefore, the steady-state positioning error is reported as approximately zero (≈0) in Table 3. The main differences among the three control strategies are reflected in the magnitude of position overshoot and the time required to reach a stable positioning state.

Table 3 Comparison of the dynamic performance of the three control strategies under 5 m and 8 m operating conditions

Target travel	Control strategy	Settling time / s	Overshoot / %	Maximum overshoot distance / mm	Steady-state positioning error / mm
5 m	Conventional fuzzy PID	8.0	10.0	500	≈0
	Standard PSO fuzzy PID	9.0	0	0	≈0
	Improved IPSO-fuzzy PID	5.5	0	0	≈0
8 m	Conventional fuzzy PID	12.0	6.3	504	≈0
	Standard PSO-fuzzy PID	11.5	0	0	≈0
	Improved IPSO-fuzzy PID	7.0	0	0	≈0

Note: "≈0" indicates that no obvious steady-state position deviation can be identified at the resolution of the current displacement-response plots; it does not imply an error strictly equal to 0 mm. The exact steady-state positioning error should be calculated from the original simulation data.

Under the 5m target-travel condition with a 100kg payload, Fig. 13 and Table 3 show that the conventional fuzzy PID controller ultimately drives the load platform to the target position but exhibits a pronounced position overshoot during the braking and positioning stage. The peak position is approximately 5.5m, corresponding to an overshoot of about 10%, or a maximum position overshoot distance of approximately 500mm. This indicates that the conventional fuzzy PID controller still produces a relatively large transient positioning deviation as the load platform approaches the target position.

After PSO-based parameter optimization, the standard PSO-fuzzy PID controller effectively suppresses position overshoot, reducing the maximum overshoot distance to 0mm and markedly attenuating the residual end-position oscillation. However, its settling time remains approximately 9.0s, indicating a comparatively slow response. By contrast, the improved IPSO-fuzzy PID controller maintains 0% overshoot while reducing the settling time to approximately 5.5s, which is about 3.5s shorter than that of the standard PSO-fuzzy PID controller. After the system reaches steady state, the actual load-platform position is nearly coincident with the 5m target, and no obvious steady-state positioning deviation can be resolved from the current response plot. Therefore, under the 5m, 100kg operating condition, the improved IPSO-fuzzy PID

controller preserves high end-positioning accuracy, avoids the approximately 500mm transient overshoot observed with the conventional fuzzy PID controller, and substantially shortens the time required to reach a stable positioning state.

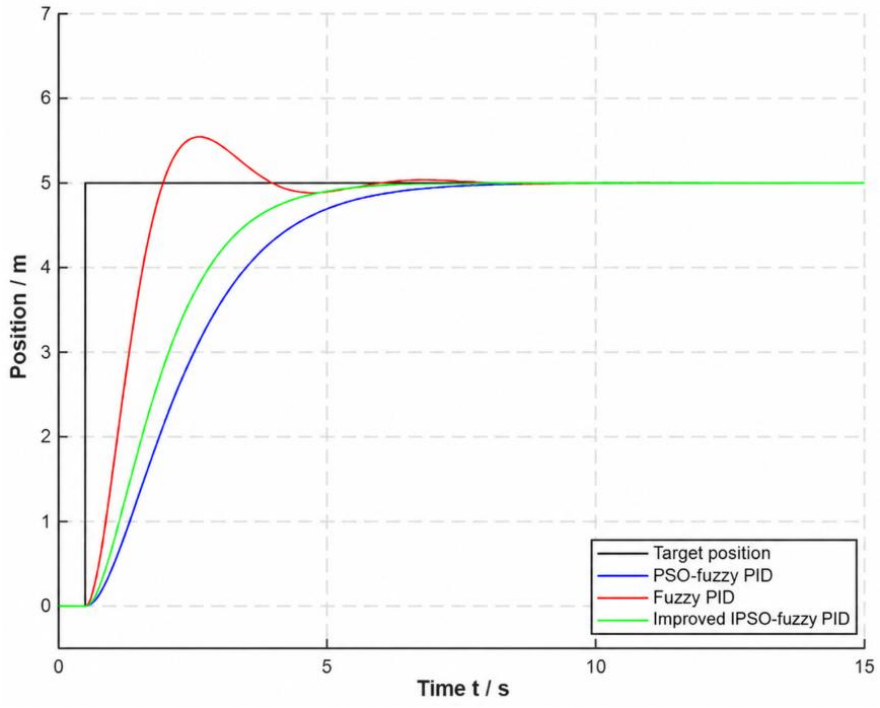


Fig. 13. Displacement response curves for the 5 m travel condition

For the long-travel operating condition with an 8 m lifting stroke and a relatively high load of 200 kg, the effects of system inertia and the dynamic disturbances associated with long-chain transmission become more pronounced as the lifting stroke and payload increase. As shown in Fig. 14 and Table 3, the conventional fuzzy PID controller exhibits a position overshoot of approximately 6.3%, corresponding to a maximum overshoot distance of about 504 mm, accompanied by prolonged dynamic oscillations and a settling time of approximately 12.0 s. The conventional PSO-based fuzzy PID controller reduces the position overshoot to 0%, corresponding to an overshoot distance of 0 mm, and effectively suppresses terminal position oscillations. However, its settling time remains approximately 11.5 s.

By contrast, the proposed improved particle swarm optimization-based fuzzy PID (IPSO-fuzzy PID) controller maintains zero position overshoot while further reducing the settling time to approximately 7.0 s, representing a reduction of about 4.5 s compared with the conventional PSO-based fuzzy PID controller. The response curves at the end of the simulation indicate that the actual position of the load-carrying platform converges steadily to the target position of 8 m, with no discernible steady-state position error at the resolution of the presented figure. Therefore, under the 8 m lifting stroke and 200 kg load condition, the proposed IPSO-fuzzy PID controller effectively eliminates the approximately 504 mm transient position overshoot observed with the conventional fuzzy PID controller while significantly shortening the positioning settling time. These results demonstrate that the proposed control strategy provides favorable terminal positioning accuracy and dynamic adaptability under the

tested long-travel and variable-load operating conditions.

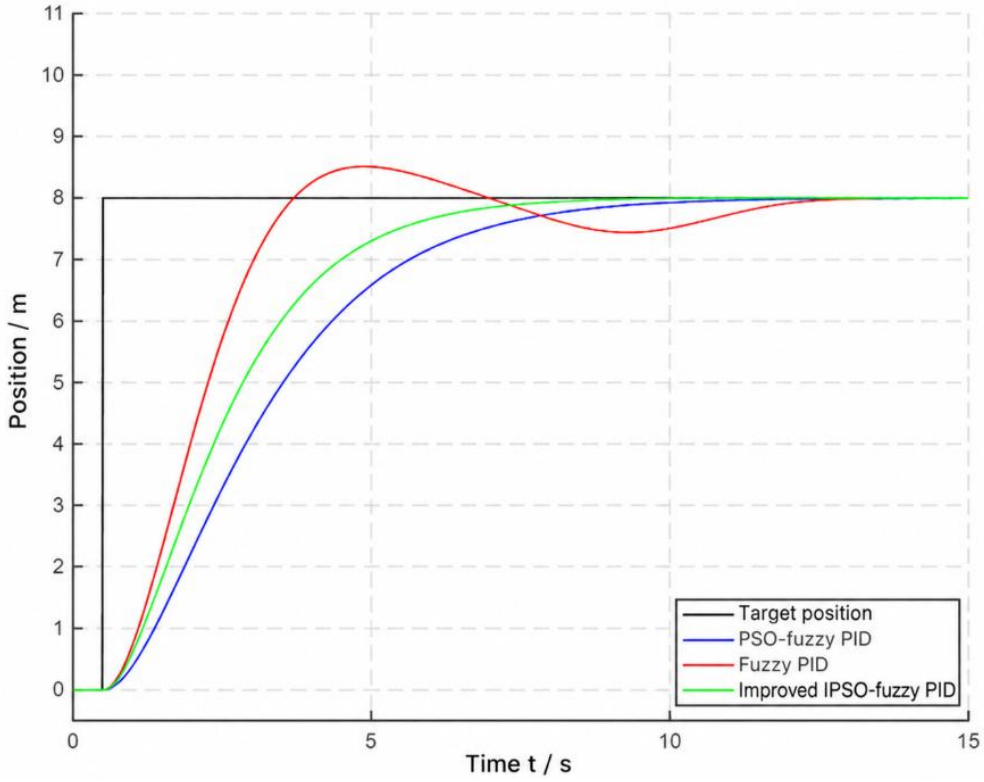


Fig. 14. Displacement response curves for the 8 m travel condition

6 Conclusions

Based on the results obtained under the two operating conditions, the conventional fuzzy PID controller can eventually achieve the desired position tracking; however, maximum transient position overshoots of approximately 500 mm and 504 mm are observed during the braking and positioning stages of the lifting mechanism, respectively. Although the conventional PSO-based fuzzy PID controller effectively suppresses position overshoot, its settling time remains relatively long. In contrast, the proposed improved particle swarm optimization-based fuzzy PID (IPSO-fuzzy PID) controller exhibits no discernible position overshoot under either operating condition, while reducing the settling times to approximately 5.5 s and 7.0 s, respectively. At the resolution of the available simulation response curves, all three control strategies eventually converge to their respective target positions, with no appreciable steady-state position errors observed. These findings indicate that the primary advantages of the proposed IPSO-fuzzy PID controller lie in its ability to effectively suppress transient position overshoot and shorten the final positioning time while maintaining a near-zero steady-state positioning error.

Declarations

Funding

This work was supported by the Shanxi Province Key Research and Development Program Project (No. 202402150101006).

Competing interests

The authors declare that they have no known competing financial interests or personal relationships that could have appeared to influence the work reported in this paper.

Ethics approval

This study did not involve human participants, human data, or animal experiments. Therefore, ethical approval was not required.

Consent to participate

Not applicable.

Consent for publication

Not applicable.

Availability of data and materials

The simulation data supporting the findings of this study, including the Adams-Simulink co-simulation results and controller performance evaluation data, are available from the corresponding author upon reasonable request.

Author contributions

Mingliang Yang conceived and supervised the research. He provided guidance on the control strategy and overall research framework.

Jiaming Xu developed the methodology, established the Adams-Simulink co-simulation model, designed the IPSO-based fuzzy PID controller, performed the simulations, analyzed the results, and wrote the manuscript.

Xijun Xu and Heng Yang contributed to the optimization algorithm design, model construction, and validation of the simulation results.

Qing Dong contributed to the data analysis, manuscript revision, and improvement of the presentation.

All authors reviewed and approved the final manuscript.

Acknowledgements

The authors would like to thank the editors and reviewers for their valuable comments and suggestions, which helped improve the quality of this manuscript.

Clinical trial registration

Not applicable. This study did not involve a clinical trial.

References

[1] Zhang Y, Liu L, Ke C, et al. Overhead crane control system based on improved dua l-loop fuzzy PID control algorithm. *Journal of Fujian University of Technology*. 2024; 22(3):258–266. https://doi.org/10.3969/j.issn.2097-3853.2024.03.008 (in Chinese).

[2] Li H, Hui Y, Ma J, et al. Research on variable universe fuzzy multi-parameter self-t uning PID control of bridge crane. *Applied Sciences*. 2023;13(8):4830. https://doi.org/1 0.3390/app13084830.

[3] Wang W, Yang Z, Zhao X, et al. Research on hydraulic tension fuzzy-PID control te chnology of mine belt conveyor. Coal Science and Technology. 2024;52(3):217–224. https://doi.org/10.12438/cst.2023-0597 (in Chinese).

[4] Liu Y, Jiang H, Zhang X. Fuzzy PID constant force control based on PSO optimizati on. Electronic Measurement Technology. 2023;46(9):16–22. https://doi.org/10.19651/j.cn ki.emt.2211068 (in Chinese).

[5] He K, Chen J, Pan F, et al. Adaptive negative-pressure control system for electric-dri ven seeding blowers based on a DILPSO-fuzzy PID controller. Computers and Electro nics in Agriculture. 2025;239:110833. https://doi.org/10.1016/j.compag.2025.110833.

[6] Liu D, Zhao S, Zhang J. Adaptive PID control of hydropower units based on particle swarm optimization and fuzzy inference. Water. 2025;17(10):1512. https://doi.org/10.3 390/w17101512.

[7] Hailu GL, Yatayew TT. Intelligent trajectory tracking in autonomous plantation robots using PSO-tuned nonlinear fuzzy PID, fuzzy PID, and conventional PID controllers. Scientific Reports. 2025;15:45357. https://doi.org/10.1038/s41598-025-30167-2.

[8] Kennedy J, Eberhart R. Particle swarm optimization. In: Proceedings of the IEEE Inte rnational Conference on Neural Networks (ICNN'95); 1995 Nov 27–Dec 1; Perth, W A, Australia. IEEE; 1995. p. 1942–1948. https://doi.org/10.1109/ICNN.1995.488968.

[9] Yang X, Cao Y, Li T, et al. Bridge crane co-simulation based on SolidWorks/Adams /MATLAB. In: Proceedings of the 2023 9th International Conference on Virtual Reali ty (ICVR). IEEE; 2023. p. 309–314. https://doi.org/10.1109/ICVR57957.2023.10169531.